POWER GENERATION ON THE ROTATING FRAME FOR HELICOPTER ICE PROTECTION SYSTEMS

Luigi Bottasso, Leonardo Helicopters, Technology & Innovation, Cascina Costa (VA), Italy
Alessandro Bazzi, Servotecnica SpA, Nova Milanese (MB), Italy
Enrico Morelli, Motom Srl, Zanica (BG), Italy
Giorgio Dalla Costa, Italwatt Srl, Leini (TO), Italy

Abstract

Helicopters operating in meteorological conditions that can lead to ice formation need an ice protection system (IPS). Current anti-icing technology relies on electrical heaters embedded in the rotor blades and the IPS shall ensure the reliable delivery of tens of kW of electrical power to the helicopter's rotors to melt the ice or prevent its accretion. The standard solution entails power generation on the airframe and subsequent distribution to the rotors by means of dedicated mechanical and electrical subsystems distributed within the rotorcraft. This solution is sub-optimal because the system's installation requires substantial modifications to the baseline helicopter, leading to higher weight, complexity, cost and maintenance. In the present work, we present an alternative "plug-in" approach where the IPS consists of self-contained modules that can be installed or removed with minimal impact, like a kit. Synchronous, brushless alternators generate the required power directly where needed, thus leading to overall system simplification. We developed, manufactured and rig-tested a demonstrator of this concept applied to a helicopter tail rotor. The chosen generator layout is a radial flux type, packaged with its electronics control and distribution sub-systems into a slip ring-type form factor. Preliminary tests were performed in a lab environment while full-scale validation took place on a tail rotor rig. We also conducted preliminary studies toward a main rotor application that represents a more challenging use case, mainly due to the need to speed-up the generator through a gearbox.

1. INTRODUCTION

The goal of the proposed paper is to present the design, development, manufacturing and test of a self-contained power module aimed at producing electrical energy directly at point of use on the rotating frame of a helicopter rotor. We propose this novel approach as an alternative to the transfer of electrical power through slip rings, which represents the common practice. The use case demonstrated in the present work is the ice protection system (IPS) of a helicopter rotor (Figure 1), though other applications of the technology are conceivable, e.g. active blade control for vibration reduction, rotor morphing or any other case where substantial electrical power is required on a rotating frame. The proposed system architecture generates power directly where needed through permanent magnet, synchronous, brushless machines. The approach aims at reducing system complexity, the weight of distribution units and

Figure 1: IPS-equipped helicopter

Presented at the 51st European Rotorcraft Forum, 9-12th September, 2025 in Venice, Italy

associated cabling, and at minimizing modifications to the helicopter airframe. It could also provide increased available power levels compared to state of the art solutions. The nominal application use case considered in the paper is the electrical power generation for the IPS of a notional twin-turboshaft helicopter. The installation of the IPS is required when a helicopter shall be able to operate in conditions leading to risk of ice accretion.

The IPS comprises generators, transformers, distribution and control units, cabling, slip rings and electrical heaters deployed in various critical areas of the helicopter such as windscreens, pitot tubes, engine intakes and, above all, rotor blades. The latter absorb by far the largest fraction of the power. A typical IPS includes dedicated generators rated at several tens of kVA. The generators' AC output is converted into 270 V DC before being fed to the slip rings and then to the blade heaters. The DC conversion is not a requirement of the IPS function as such, rather it is easier to feed in DC multiple loads and connect multiple DC power supplies in parallel (see refs. 1, 2 for an overview of ice protection systems for rotorcraft). Although both main and tail rotors of a helicopter can benefit from this novel in-situ power generation technology, the higher rpm of the tail rotor are more suitable for a direct-drive application.

Wind-turbine drivetrains are similar to our application, though "inverted" because in the wind energy case the magnets are on the rotor side, e.g. see ref. 3.

Acronyms:

ADC	Analog-to-Digital Converter
BERC	Banco Elettrico Rotore di Coda
ECS	Environmental Control System
EEPROM	Electrically Erasable Programmable ROM
IGBT	Insulated-Gate Bipolar Transistor
IPS	Ice Protection System
MGB	Main Gear Box
MR/TR	Main/Tail Rotor
NTC	Negative Temperature Coefficient
OAT	Outside Air Temperature
PM	Permanent Magnet
SCR	Silicon Controlled Rectifier
SPI	Serial Peripheral Interface
TGB	Tail Gear Box

2. RATIONALE

The present work describes a project performed by Leonardo Helicopters Division (LHD) encompassing feasibility study, detailed design, manufacture and test of a tail rotor IPS based on a brushless generator with permanent magnets for a notional helicopter.

A typical IPS is quite complex and requires ice detectors, air temperature sensors, transformer and rectifier units, electrical power distribution and control units, slip rings for main and tail rotors as shown in Figure 2. Considering also the wiring, status panels, circuit breakers and the various structural support provisions, the overall system mass can exceed 200 kg. Furthermore, the presence of the above-mentioned IPS generators entails dedicated provisions in the main gearbox and imposes trade-offs, e.g. the ECS (Environmental Control System) compressor unit cannot be installed due to lack of available space around the helicopter's main gearbox (MGB) on which the generators are mounted. Therefore, IPS-equipped helicopters cannot have air conditioning.

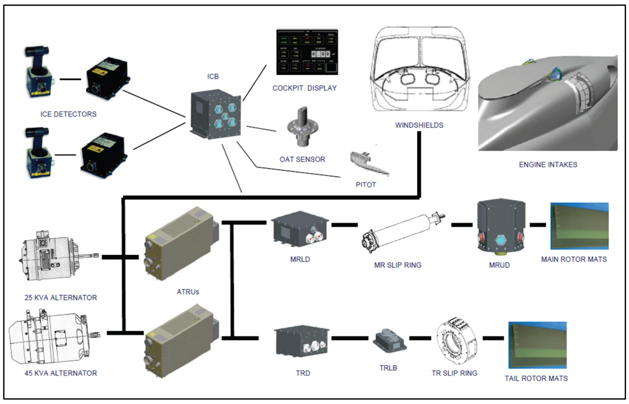

Figure 2: Components of the legacy IPS

Another aspect is the fact that current slip rings require maintenance due to brush wear.

The alternative that we explored in the present work is the adoption of a radically different system architecture where electrical power, instead of being generated on the airframe, is provided at point of use with brushless machines.

The benefits consist in the overall system simplification, lower weight, less component wear and possibly lower maintenance costs. The local distribution reduces the weight of cabling and the contactless design eliminates friction-induced degradation, while at the same time protecting against lighting and arching because the air-gap acts as an insulator.

An accurate evaluation of the weight reduction potential of the new system architecture is beyond the scope of work. However, we performed a preliminary assessment of the system requirements compared to the current list of typical IPS system components.

Presented at the 51st European Rotorcraft Forum, 9-12th September, 2025 in Venice, Italy

Considering the items that would become unnecessary and those that could be reduced (e.g. the numerous structural supports and wiring provisions) a net weight saving of up to 30% appears to be potentially achievable. Figure 3 illustrates the overarching concept of the new IPS architecture.

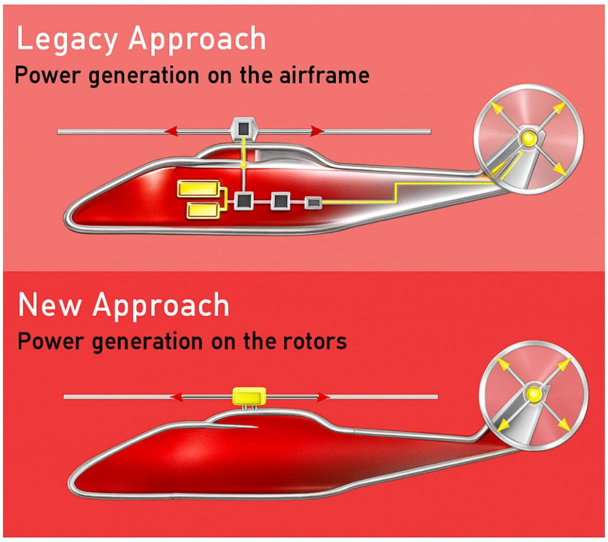

Figure 3: The new streamlined IPS architecture

There are two possible ways to perform the ice protection function: de-icing and anti-icing. In the de-icing scenario, the system allows some ice accretion to occur on the rotor blades and then applies heat to remove the ice through a cycling schedule across different heater mat elements embedded in each blade. A typical main rotor IPS employs this scheme because the power requirement is relatively low, in the order of 20-25 kW.

Conversely, the anti-icing approach aims at heating the blades continuously in order to prevent ice formation in the first place. In principle, this is preferable and safer than de-icing, however, the drawback is a much higher power demand compared to de-icing. This is acceptable on the smaller tail rotor, though.

An electrical machine installed on the main rotor, spun with adequate rpm, could release high power levels with very low transmission losses. Therefore, a possibility offered by local power generation consists in shifting from a de-icing to an anti-icing logic even on the main rotor. A further aspect to consider is the ability to power the IPS in AC, which would avoid the losses inherent in AC/DC conversion while at the same time eliminating the weight of the transformer and rectifier units of the legacy system.

A key parameter affecting the performance of electrical machines, be they radial or axial flux types, is the rotational speed differential between rotor and stator. Electrical machine design favors higher speed because less torque is required for a given output power, leading to higher power-to-weight ratios. Less torque in turn translates into a more compact and lighter design (e.g. for an axial flux topology, torque depends roughly on $D^{3.5}$, where D is the machine diameter,). The above factors lead to different design choices for main and tail rotors. A typical main rotor nominal rotational speed is a few hundred rpm, which is not very fast for an electrical machine. In this case, it is necessary to accelerate rotor / stator relative speed through a gearbox; there are several ways to achieve this. Hereafter we present and illustrate, through notional schemes, three alternative main rotor applications analyzed mainly in terms of transmission kinematics architecture.

The first, shown in Figure 4, involves the use of an epicyclic gearbox to speed-up the rotors in a counter-

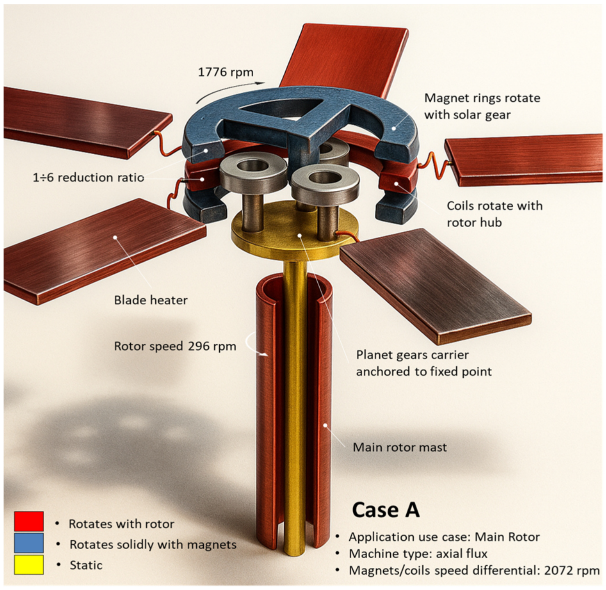

Figure 4: Main Rotor - Case A)

rotating architecture. In this case, the planetary carrier stage acts as the “fixed frame” anchored through a centerline shaft coaxial to the main rotor mast.

The solar gear drives the permanent magnets, while the external ring gear is fixed to the rotor hub together with the coils generating electrical power for the blades. Gearbox lubrication could be performed with grease or splash lubrication because feeding pressurized oil to a rotating frame would be impractical.

Considering a notional main rotor speed of 296 rpm, and assuming a ratio of 1:6 between ring and solar gears in the epicyclic stage, a rotational speed differential of 2072 rpm between magnets and coils could be achieved with this architecture.

As an alternative, the discs carrying the permanent magnets could be attached to a rotating shaft connected to the MGB solar gear. Assuming a solar gear rotational speed of around 1355 rpm in the same direction as the rotor (296 rpm), the layout would provide a differential speed of 1059 rpm between rotor and stator. This solution represents a trade-off which eliminates the dedicated gearbox but at the cost of slower speed. Figure 5 illustrates the scheme.

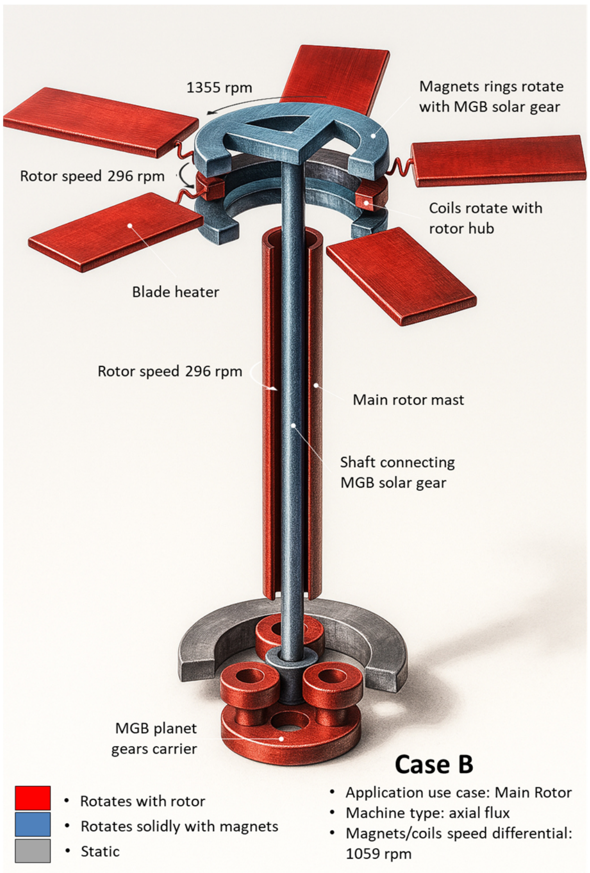

Figure 5: Main Rotor - Case B)

A third option consists in combining the gearbox of case A) with the shaft rising from the MGB solar gear of case B); but with the shaft now driving the planet carrier of the epicyclic gear as illustrated in Figure 6 (again, with a gear ratio 1:6). This configuration is the most effective, producing a speed differential of 7413 rpm between rotor and stator.

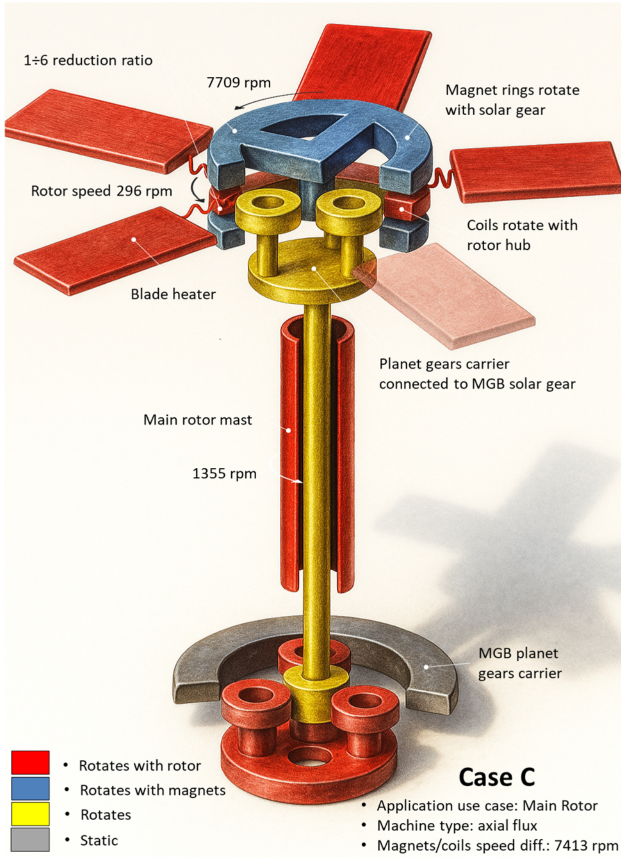

Figure 6: Main Rotor - Case C)

Table 1 summarizes the results of a conceptual pre-sizing of the active parts of a notional axial flux generator for the different use cases described above.

Table 1: sizing of a notional axial flux generator for main rotor IPS application (active parts only)

Function	Case	Power required (kW)	Speed (rpm)	Active parts mass (estimate) (kg)
De-icing	A	20	2072	14
	B	20	1059	21
	C	20	7413	7
Anti-icing	A	65	2072	20
	B	65	1059	45
	C	65	7413	14

Building on the previous points, Figure 7 aims at illustrating a vision of case C) through a schematic view of a complete main rotor IPS generator in the 60-70 kW range, thus suitable for an anti-icing function. Here, the rotor beanie encapsulates an integrated module with axial flux generator, gearbox, control electronics and radiators to dissipate excess heat.

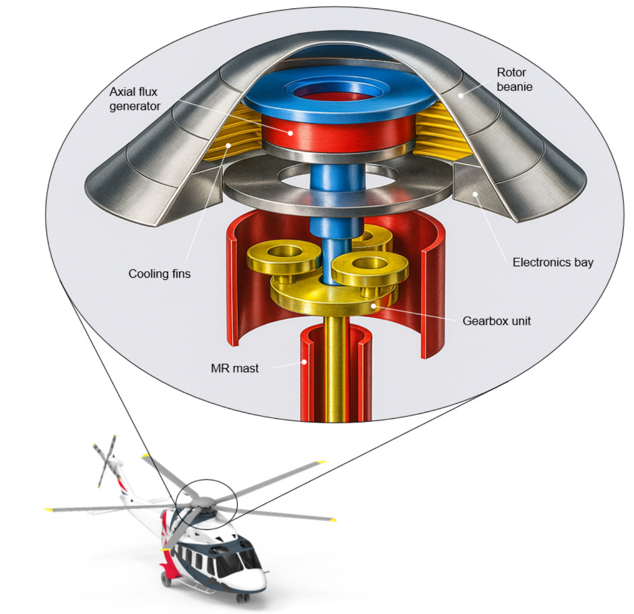

Figure 7: Artist's impression of an IPS based on the scheme of case C), integrated into a MR beanie

The tail rotor application use case is somewhat easier than the main rotor because here we can adopt a direct-drive approach due to the higher rotational speed, in the order of 1400-1500 rpm (Figure 8). The

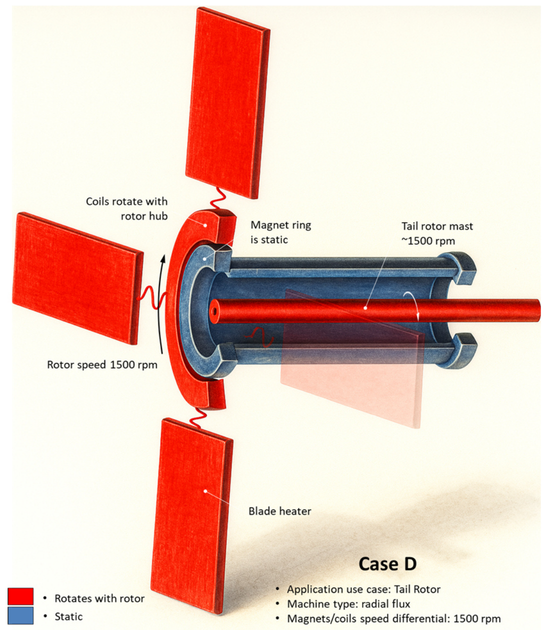

Figure 8: Tail Rotor - Case D)

paper describes this use case, implemented up to prototype manufacturing and testing @TRL6.

Leonardo Helicopters holds a cluster of granted patents related to both main and tail rotor concepts, patents that were developed, filed and published over the past years in parallel with design and development activities; see ref. 4-6. We take the opportunity to remark that differences exist between the innovations disclosed by the patents and the actual hardware that was developed.

As an example of these deviations, the generator configuration that we designed and built for the present work has a radial flux topology because it is more suitable for assembly/disassembly of the rotor and stator, while the patents describe axial flux machines. For a comparison of axial and radial machines, see ref. 7.

3. SYSTEM ARCHITECTURE

Unlike standard slip rings, our concept involves electrical machines where stator and rotor are physically separated from each other, i.e. not only the electromagnetic design is brushless, but also the mechanical design is bearingless. Figures 9 and 10 show at conceptual level the relative position of the machine's rotor with respect to the stator in the TR use case.

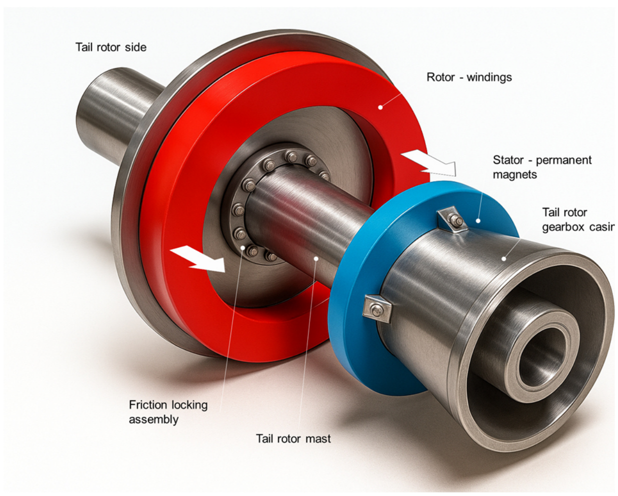

Figure 9: Schematic assembly of the TR generator

The rotor side of the generator (red), which is the part carrying the coils that feed current to the blades, is locked in place on the TR mast through a friction-locking flange compressed through conical rings, performing various functions: load reaction, rotor/stator mutual alignment and air gap safeguarding.

The stator (blue) is bolted on the tail rotor gearbox casing and has the permanent magnets arranged on its perimeter. The absence of all sorts of rolling and sliding contacts is supposed to alleviate one of the key disadvantages of the slip rings, i.e. their maintenance burden.

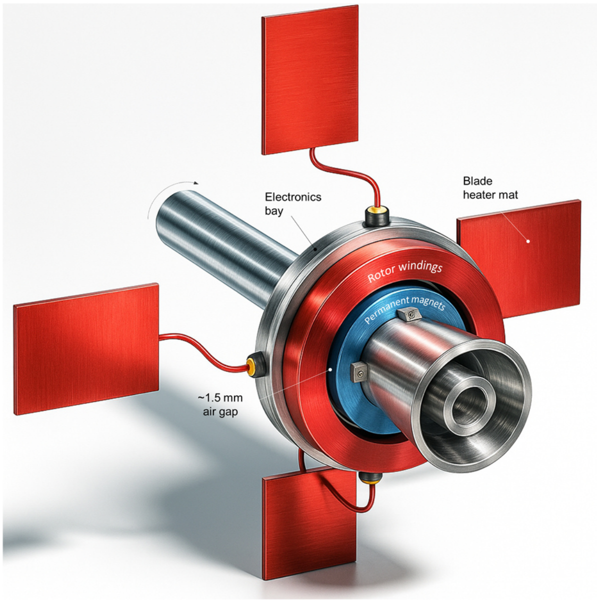

Figure 10: Assembled configuration of the TR generator scheme shown in Figure 9

Slip ring brush replacement, bearing inspection and repair can require the removal of the complete rotor.

There are several advantages associated with the use of permanent magnets in electrical machines. First of all the magnets do not require the supply of current so there is no need to run cables, leading to simpler, lighter design, but also reduced Joule losses and higher efficiency: up to 97% vs 90-93% for induction machines. Furthermore, rare earth magnets have high field (1.32 T for the NdFeB magnets used in the project) leading to high torque density.

3.1. Machine design

The chosen machine design is a three-phase permanent-magnet alternator.

The electrical load of the notional TR IPS analyzed is composed of four resistors of 10.5 Ohm, one for each rotor blade. We assumed a four-bladed tail rotor having a FIPS electrical topology with opposite blades connected in series and, in turn, the two pairs in parallel. Therefore each of the two resistance branches has approximately 21 Ohm each, in parallel to obtain approximately 10.5 Ohm.

In order to replicate the interfaces of current system we decided to rectify and feed 270 Vdc to the rotor blades; but this is not a mandatory requirement and could be simplified in future designs. The power output of the alternator (between 100% = 1379 rpm and 105% = 1448 rpm) is:

- 230-240 Hz
- 290-300 Vdc (then stabilized @ 270 Vdc)
- 28-29 Adc
- 7.5-8 kW

The power dissipated in the resistors is thus approximately 8 kW with a tail rotor operating speed Ω = 1448 rpm and environmental temperature range T = -40°C / +20°C. The design had to respect strict volume constraints and air-gap allowances due to the geometry of the tail rotor hub and the articulated blades that can oscillate during operation by several degrees around lead-lag, flapping and pitch hinges. A magnetic air gap of 2 mm was chosen; the actual mechanical gap is 1.5 mm due to magnet wrap taping.

Despite the fact that permanent magnets are subject to brittle failure behavior, they provide the previously mentioned benefits. In particular, we selected Neodymium NdFeB rare earth magnets (shown in Figure 11) due to their exceptional performance in terms of magnetic flux density.

Figure 11: A pair of NdFeB permanent magnets used on the alternator's stator

As an alternative to NdFeB, we also considered PMs based on Sm2Co17. Samarium Cobalt magnets have the advantage of better temperature stability and are also suitable for higher operating temperatures up to 350°C, though their maximum magnetic field is somewhat lower. These magnets have also greater corrosion resistance compared to NdFeB.

Eventually, the choice of Neodymium magnets was justified because thermal analyses showed that maximum temperatures in the magnets would never become excessive even under worst-case scenarios. Based on the operational characteristics, volume and mass constraints, the machine configuration that was considered most suitable for our application is a

Presented at the 51st European Rotorcraft Forum, 9-12th September, 2025 in Venice, Italy

three-phase sinusoidal synchronous machine with radial field. This type of machine allows the adoption of a sufficiently large number of poles, reducing the sections of the magnetic field yokes. The machine has an inductor with 20 permanent magnets poles and a 24-slot rotor with three-phase windings. To evaluate the performance of the alternator, non-linear electromagnetic and thermal FEM analyses were performed, as shown in Figure 12, while the actual stator and rotor are illustrated in Figure 13.

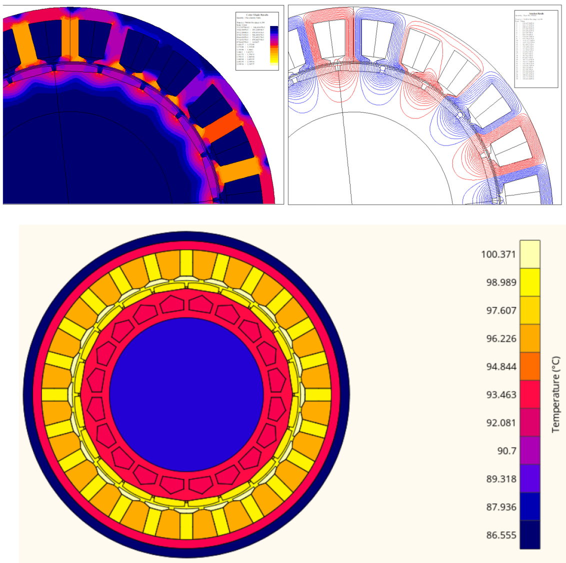

Figure 12: Electromagnetic and thermal model plots

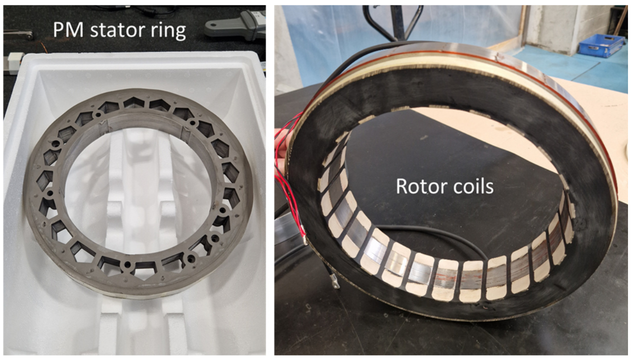

Figure 13: The main components of the alternator

Electromagnetic simulations were performed for the conditions listed in Table 2, for different rotational speeds and assuming an external ambient temperature OAT = 5 °C with varying airflow speeds acting as forced convection cooling. This is realistic since the IPS is used when the atmospheric conditions are prone to icing and therefore the external temperature is close to or below freezing point. This factor, combined with the rotor-induced air inflow, naturally contributes to machine cooling. Some runs were also performed at OAT = 20 °C and no airflow. We assumed two separate thermal conditions for the machine: given that the active parts of the generator should not exceed 100 °C for safe operation, a first set of cases was analyzed where magnetic induction Br and resistivity R are calculated at T = 100 °C. Furthermore, Br and R values calculated at T = 20 °C were used in a second set of simulations because at this temperature the voltage reaches a maximum, and this is the voltage level that needed to be taken into account as a worst case scenario for the electronics design.

In order to evaluate failure scenarios, a complete three-phase short circuit was conservatively assumed in the simulations. The results show that no demagnetization occurs in the magnets for T = 20 °C, while for T = 100 °C a tiny portion of a permanent magnet is subject to demagnetization. The resulting maximum braking torque resulting from short-circuit simulations is equal to 205 Nm.

Table 2: The electromagnetic and thermal conditions modelled in the simulations (EM = Electro Magnetic, TH = Thermal)

Cond.	RPM	Analysis	OAT (°C)	Br & R (°C)	Airflow (m/s)	Under load
Operational	1379	EM+TH	5	20	100	Yes, output stabilized @ 270V DC
			20		0	
		EM	-	100	-	
	1436	EM+TH	5	20	100	
					80	
					60	
					40	
					20	
					15	
					10	
					5	
					0	
			20		0	
		EM	-	100	-	
Non oper.	1837	EM+TH	5	20	100	No
			20		0	
		EM	-	100	-	
Short circuit	-	EM	-	20	-	Yes
				100		

The results show that all conditions analyzed are tolerable by the machine, both from a performance and from a thermal point of view. Different conditions were analyzed where the alternator generates its nominal power under various level of forced convection cooling. The thermal exchange is of crucial importance because the models show that natural convection alone would lead to temperatures reaching a value of 126 °C in the active parts, well above the recommended limit.

Presented at the 51st European Rotorcraft Forum, 9-12th September, 2025 in Venice, Italy

Extensive simulation proved that even a moderate airflow, in the 20-40 m/s speed range, is enough to contain the thermal load within acceptable levels.

The assessment of the direct effects of lightning is not applicable to the study of the generator because the machine is contained within a metal shell. However, the component's insulation system was designed to comply with 2 kV stiffness test and guarantees an insulation of at least 20 MΩ at 500 V.

3.2. Electrical / electronic design

The electrical circuit schematic diagram is illustrated in Figure 14. The three phases of the generator, after being rectified by a half-controlled bridge rectifier, feed two resistors in parallel. Each of them represents the heater mats of a pair of opposite blades connected in series. Voltage and current sensing is transmitted to the central processor for monitoring purposes.

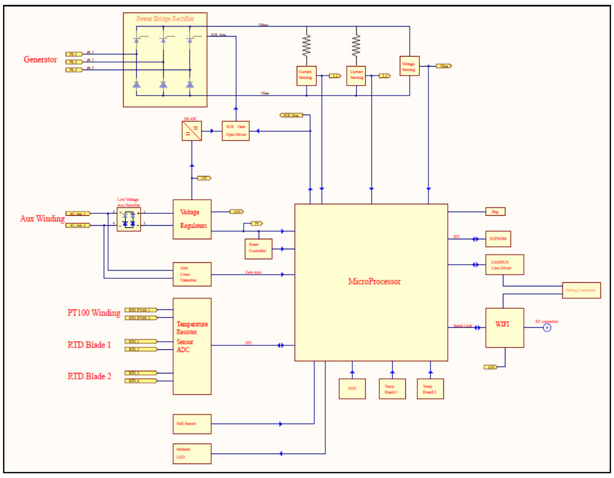

Figure 14: Electrical circuit diagram of the generator

Two auxiliary windings provide 25 Vrms single-phase voltage @ 1379 rpm with a sinusoidal waveform. This is then converted to 15 Vdc and a current of approximately 350 mA to power the electronic board. In the speed range 1000 - 1250 rpm, the auxiliary windings guarantee stable 15 Vdc even with the LEDs on, both with and w/o power load. Auxiliary power also enables on/off switching of the generator through an optical SCR gate. Thermocouples embedded within the blade heater mats send their signals to the microcontroller through ADC analog-to-digital sensors. SPI serial protocol is used, as is standard in embedded systems for short-distance wired communication between integrated circuits. Control logic within the microcontroller ensures that the generator is switched off before blade overheating occurs. The ADC can also read external sensors, if needed. The electronics PCB is visible in Figure 15 that illustrates the generator with the front cover open; red resin was applied on soldered connections to make them more ruggedized against centrifugal acceleration and vibrations.

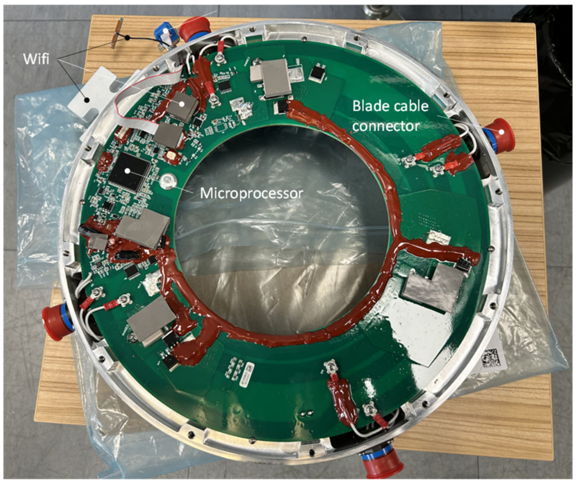

Figure 15: The generator with the front cover open

Due to the contactless nature of the machine, LEDs / photodiode and Hall sensor / coil ensure two-way communication between rotating and fixed frames. The Hall sensor shown in Figure 16 is powered through 12 Vdc, 5A.

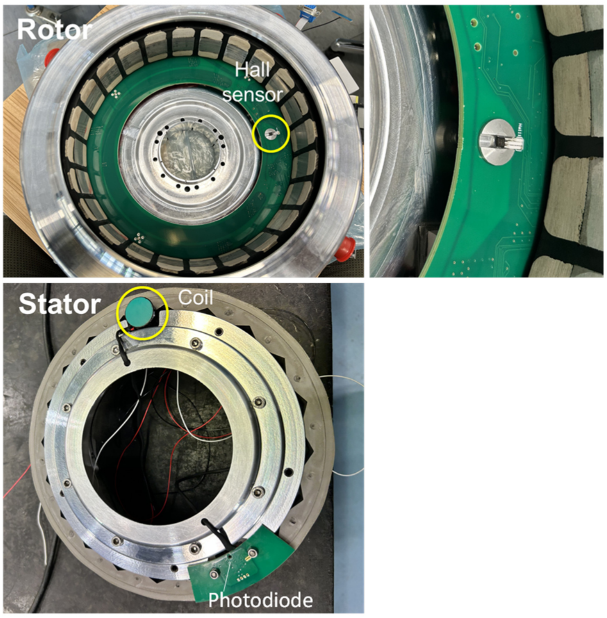

Figure 16: Hall sensor on the back of the PCB within the rotor (above), activation coil on stator (below)

The Hall-effect sensor provides the on/off function, while a pair of infrared LEDs provide wireless transmission of the system status signal (on/off) from the rotating to the fixed frame. The LEDs can also be used to measure rotational speed or transmit more complex signals such as the readout of the blade temperature sensors.

A NTC thermistor acts as a temperature detection and compensation / protection device; in case of temperature increase its resistivity decreases to prevent damage to the electronics.

Lookup tables are programmed with appropriate temperature vs. voltage laws to be used for temperature conversion of the blade sensors. An external port is provided for software debug, e.g. to upload different blade thermal management logics and thresholds. An EEPROM memory module stores data acquired by the system. A wireless module and the associated antenna ensure real-time data streaming from rotating to fixed frame e.g. temperature for monitoring purposes during tests.

3.3. Mechanical design

Figure 17 illustrates the CAD model and the as-built generator unit showing the stator side with its four attachment points to the tail rotor gearbox and the rotor side provided with a friction flange acting as the connection to the rotor mast. Two removable connection brackets ensure mechanical coupling and alignment between rotor and stator during storage, transportation and installation.

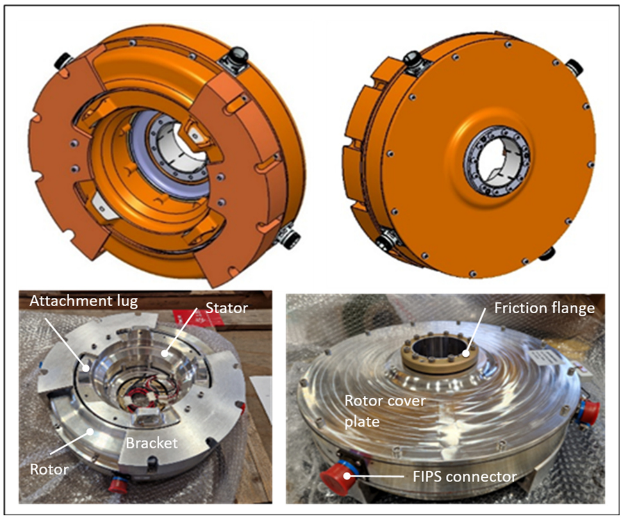

Figure 17: Complete stator / rotor assembly and associated CAD model

4. TESTING

We performed tests on the alternator and its sub-systems in two separate phases: first through the use a modified CNC machine adapted as a spinning rig, then on the BERC test rig, an outdoor facility consisting of a full-scale helicopter tail boom and rotor located at LHD facilities in Cascina Costa.

4.1. Phase 1: basic functionality test

The scope of the first set of tests was a general validation of the system's performance within a controlled environment. In this test, the electronics board was electrically connected but physically separated from the machine, in a sort of tabletop setup. For practical reasons, these tests were performed by spinning the magnets and keeping the coils and electronics board stationary, thus the machine was in an inverted configuration compared to the real operational conditions. The coils were lying on the mill bed while the magnets were driven by the CNC spindle, as shown in Figure 18. This configuration was necessary in order to be able to monitor currents and other electrical parameters of the generator from a stationary position. Obviously, this setup could not replicate the centrifugal load and vibration level expected under real conditions on the active parts of the generator and its electronics. Figure 18 also shows how the electrical heater configuration of a four-bladed tail rotor was simulated through tabletop resistors. We built two resistor branches of approximately 21 Ω each (as in opposite blade pairs of the actual rotor), in parallel to obtain approximately 10.5 Ω.

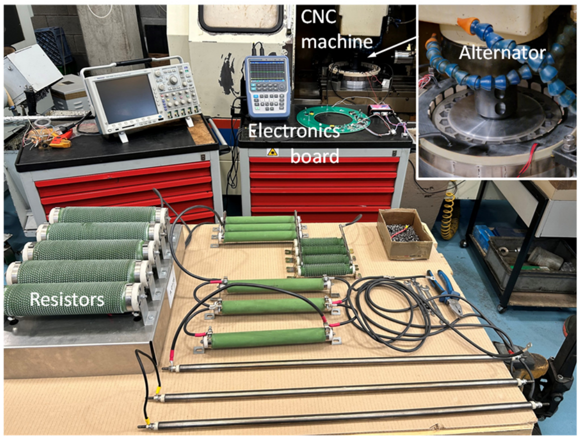

Figure 18: The rig setup used for functionality test

Different types of resistors were used to reach the desired resistance value, most were ceramic-type capable of dissipating around 300-500 W each. The main purpose of the activity was to carry out an initial check of the alternator and its electronics, to preempt at least any major electrical malfunctions once installed. Thanks to this preliminary test, we discovered a risk of overvoltage. This can happen when the alternator builds up energy that is suddenly released. The electronics board included recirculation diodes positioned at the IGBT switch precisely to prevent this phenomenon; eventually the IGBT was replaced by Thyristor/SCR to mitigate the issue more effectively during switch-on/off. A PT100 thermal probe (a 100 Ω platinum resistor) connected in open air simulated the blade temperature reading. We thus verified that the software could read the temperatures from the sensors embedded in the blades. Figures 19, 20 and 21 illustrate the dependence of Voltage, Current and Power output from rotational speed, confirming the machine ability to generate the required power levels.

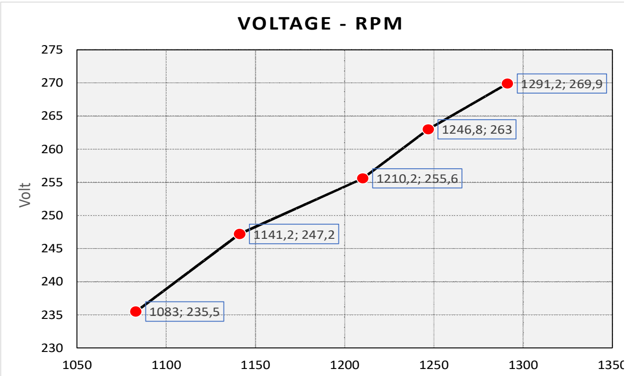

Figure 19: Voltage output vs speed

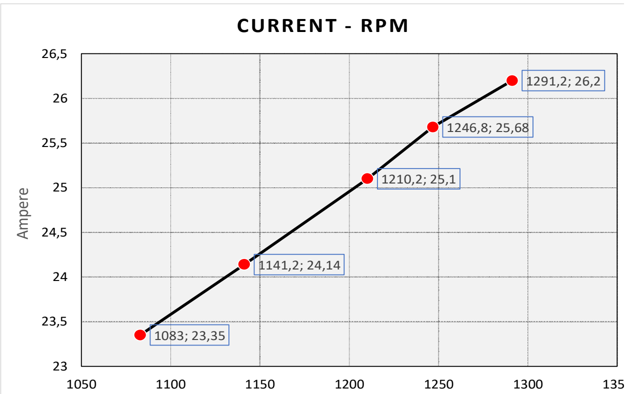

Figure 20: Current vs speed

The maximum practical speed of the CNC machine was limited to ~1300 rpm, slightly short of the 1379 rpm nominal speed of the BERC tail rotor rig.

We confirmed that 1083 rpm (~80% of nominal) is the minimum speed that guarantees stable power from the auxiliary coils to the electronics PCB; this is well below the minimum operating speed of the tail rotor. Oscilloscopes were used to monitor voltage fluctuations during switching on/off cycles, confirming the absence of over-voltages (see Figure 22).

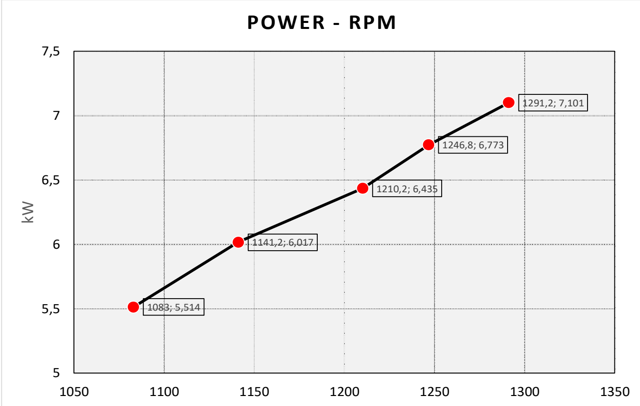

Figure 21: Power output vs speed

Table 3 lists the test points that were performed, showing that no anomalous behavior was observed.

Table 3: Basic functionality test points

Speed (rpm)	Note
1083	Minimum speed value for stable auxiliary power ON / OFF transient without overvoltage
1141	Fully functional auxiliary power to electronics PCB ON / OFF transient without overvoltage
1210	
1247	
1291	

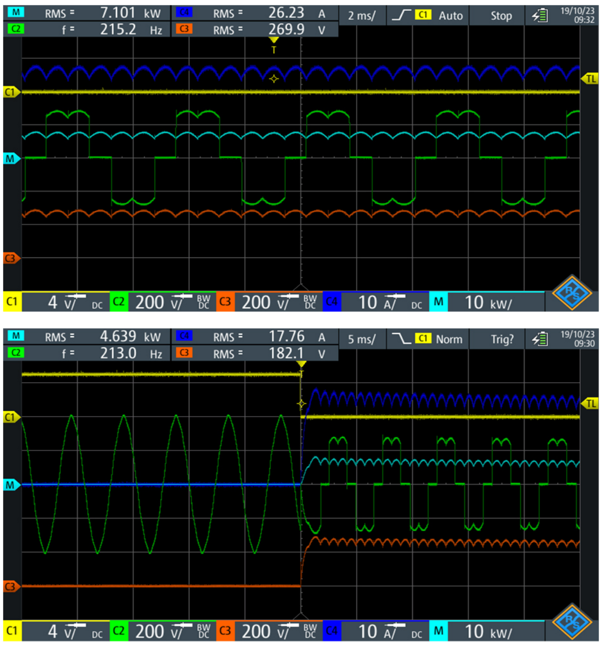

Figure 22: Oscilloscope readings in steady state @1291.2 rpm (above) and transient modes (below)

The Hall sensor and the associated coil were separately tested, indicating a minimum activation current of 3A DC and a nominal value of 5A DC.

4.2. Phase 2: full-scale test on TR rig

The second set of tests aimed at full-scale experimental validation of the system in a relevant environment, i.e. at TRL6. For this purpose, we used the BERC (Banco Elettrico Rotore di Coda - Tail Rotor Electrical Rig), a test facility based at Leonardo Helicopters in Cascina Costa, illustrated in Figure 23.

Figure 23: The BERC test rig

The rig consists in an instrumented helicopter tail boom and associated rotor drive train, powered by an electric motor, able to replicate certain aspects of real flight conditions, including rotor blade pitch change, thrust, vibration and heating of actual FIPS-equipped blades. Figure 24 shows the generator during installation on the tail rotor, while Figure 25 shows the unit after the installation of the rotor assembly and the electrical connection to the rotor blades.

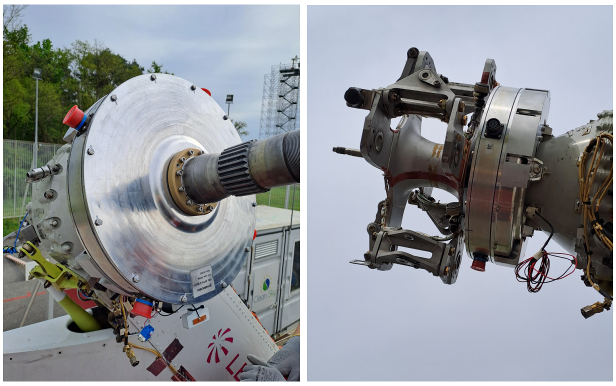

Figure 24: Alternator installed on mast (left) and after rotor hub insertion (right). Note friction flange (left)

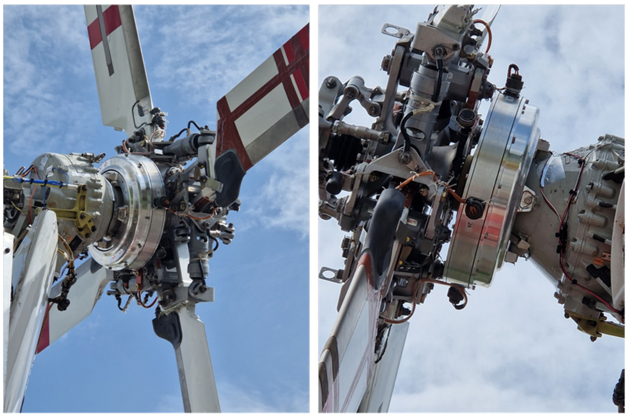

Figure 25: Alternator connected to the FIPS blades

Planned tests included the validation of the power generation capability of the TR alternator, the mechanical soundness of its design (vibration tolerance, air-gap stability, friction flange connection grip), as well as the functionality of its command and control electronics (Hall sensor for on/off switching) and LED communication unit.

Thermal strips were attached to the blades and to the generator case to register the maximum temperatures reached, while a FLIR thermal camera was used as a real-time tool to complement the temperature monitoring system embedded in the alternator electronics (Figures 26, 27).

Table 4 lists the main test conditions; note that 100% rpm corresponds to 1.379 rpm. Figure 28 shows the rotor spinning during one of the numerous runs performed in the test campaign.

Table 4: BERC test points

Run type	Speed (rpm)	Blade pitch (deg)	Time (s)	Blade heating
Rotor balancing	100%	0°/+5°	N/A	OFF
Calibration test	100%	0°	300	OFF
System functionality test 1	100%	0°/+5° -5° ↔ +10° sweep	600	Cycled on/off
System functionality test 2	102%	0°/+5° -5° ↔ +10° sweep	600	Cycled on/off
System functionality test 3	105%	0°/+5°	300	Cycled on/off
Mechanical stability test	107%	0°/+5°	300	OFF

Presented at the 51st European Rotorcraft Forum, 9-12th September, 2025 in Venice, Italy

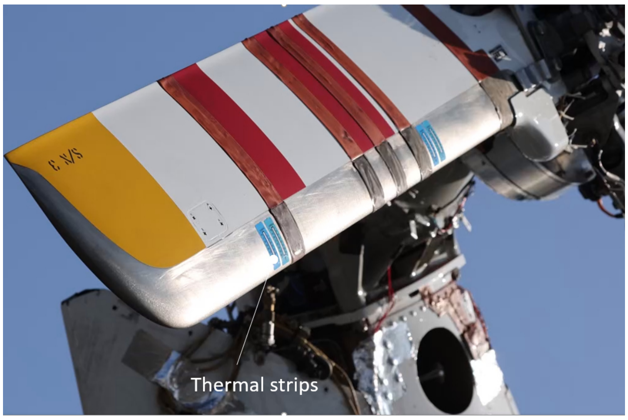

Figure 26: Thermal strips on different blade stations

Clearly, the OAT during the tests was not representative of icing conditions, as it ranged from around 17 to 25°C. This however was not an issue in the context of the tests since we aimed at validating the power generation and control performance of the alternator, knowing that the specified power output (~8 kW) was more than adequate for the IPS function.

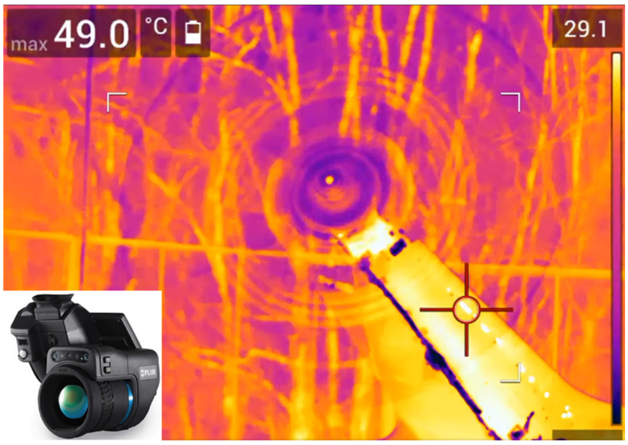

Figure 27: FLIR camera image of the spinning rotor with heated blades

The control logic used on the tail rotor during IPS operation on the real helicopter is similar to a thermostat and starts with the acquisition of external air parameters. If the air data sensors on the helicopter detect the risk of icing, then the TR blade heating is switched on until the heater mat sensor records an internal blade temperature of 55°, then the system is cycled off and on between 55° and a lower threshold of 35°. The internal temperature limit of the blade is 65° to avoid degrading the composite resin material. During tests, the alternator control system was programmed to follow the above logic, having access to the blade temperature sensor readings.

Figure 28: Test run at 102% rpm

The temperatures recorded by thermal strips attached to the blades' erosion shields is typically ~10° lower than the value recorded internally by the blade heater mat sensors. These readings were used after each run to ensure no blade overheating had occurred.

The BERC data acquisition system monitors and records test rig parameters such as rpm, blade pitch angle, stresses and xyz accelerations at different locations on the tail boom and fin. Figure 29 represents an extract of time-history plots for illustrative purposes.

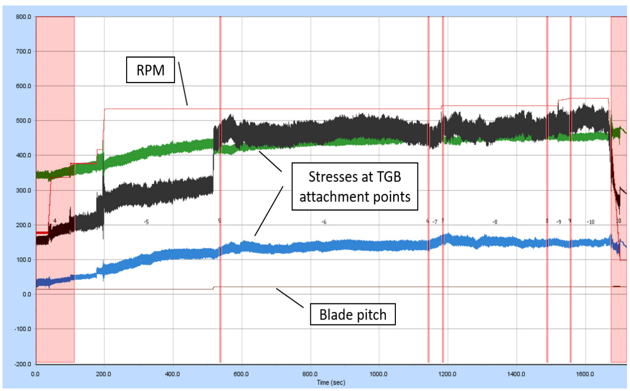

Figure 29: BERC diagnostics plots

Presented at the 51st European Rotorcraft Forum, 9-12th September, 2025 in Venice, Italy

The tests confirmed the sound design of the alternator and demonstrated the successful operation of the system including:

- Rapid blade heating capability (a few sec to reach 55° heater mat upper temperature limit)
- Automatic on/off switching on lower/upper T° thresholds
- Hall sensor functionality, on/off from fixed frame
- LED sensor status communication from rotating frame
- Mechanical stability, air-gap safeguarding
- Friction flange locking system
- Software upload/download through debug port or WiFi antenna

Regarding the last point, it was noted that WiFi protocol might need to be changed to another standard, e.g. ZigBee, to improve data transmission from rotating to fixed frames with the spinning rotor. Different antenna shapes and positions were tested to evaluate transmission quality under various conditions.

5. CONCLUSIONS

We designed, manufactured and tested the demonstrator of a next generation ice protection system for helicopter rotors. The selected use case is a tail rotor application due to the lower power need and test infrastructure availability. The vision is that of a vastly simplified IPS where power is produced at point of use through a self-contained generator module, thus greatly reducing system's weight as well as operational costs.

The machine is still at an experimental stage and is not yet fully representative of a flyable unit. Given the system's complexity and the associated risks, basic functionalities were first validated by means of a tabletop test rig and later successfully demonstrated on a notional TR use case through a real helicopter tail boom used by Leonardo as a multi-purpose test infrastructure.

We believe that the size and weight characteristics of the machine used in the TR experiment could potentially be also representative of a MR application due to the fact that in the latter case the speed would be much accelerated, making the power generation more efficient.

The novel IPS concept, if fully developed on both MR and TR, has the potential to drastically reduce system complexity and weight, the latter up to an estimated 30% compared to the current configuration, which would translate in tens of kg of weight saving.

6. ACKNOWLEDGMENTS

We take the opportunity to express our appreciation to James Wang, former Head of R&I at Agustawestland, for the concept formulation, and to Giorgio Lucchi, CEO of Lucchi R. Srl, for the knowledge and expertise that they provided.

7. REFERENCES

1. Aubert, R. J., "History of Ice Protection System Design at Bell Helicopter", FAA In-flight Icing / Ground De-icing International Conference & Exhibition, ISSN 0148-7191, June 16, 2003
2. Flemming, R. J., "A History of Ice Protection System Development at Sikorsky Aircraft", FAA In-flight Icing / Ground De-icing International Conference & Exhibition, ISSN 0148-7191, June 16, 2003
3. Stander, J.N., Venter, G. and Kamper, M.J., "Review of Direct-Drive Radial Flux Wind Turbine Generator Mechanical Design", *Wind Energy*, Vol. 15, 2012, pp. 459–472.
4. Bottasso, L., Zocchi, A., Brunetti, M., Medici, L., Wang, J. and Lucchi, G., "Aircraft Capable of Hovering With Main Rotor", European Patent - EP 3342707B1, December 30, 2016
5. Bottasso, L., Zocchi, A., Brunetti, M., Medici, L., Wang, J. and Lucchi, G., "Rotor for an Aircraft Capable of Hovering", European Patent - EP 3342705B1, December 30, 2016
6. Brunetti, M., "Rotor for an Aircraft Capable of Hovering and Relative Method", European Patent - EP 3342706B1, December 30, 2016
7. Parviainen, A., "Design of Axial-Flux Permanent-Magnet Low-Speed Machines and Performance Comparison Between Radial-Flux and Axial-Flux Machines", ISBN 952-214-029-5, 2005